Agile wavefront splitting interferometry and imaging using a digital micromirror device

La Torre, Juan Pablo, Amin, M. Junaid, Riza, Nabeel

Juan Pablo La Torre, M. Junaid Amin, Nabeel A. Riza, "Agile wavefront splitting interferometry and imaging using a digital micromirror device," Proc. SPIE 9896, Optics, Photonics and Digital Technologies for Imaging Applications IV, 98960B (29 April 2016); doi: 10.1117/12.2228373

SPIE.

Event: SPIE Photonics Europe, 2016, Brussels, Belgium

Agile Wavefront Splitting Interferometry and Imaging using a Digital Micromirror Device

Juan Pablo La Torre[a], M. Junaid Amin[a] and Nabeel A. Riza[*a],
[a]School of Engineering, University College Cork, College Road, Cork, Ireland
*Corresponding author: n.riza@ucc.ie

ABSTRACT

Since 1997, we have proposed and demonstrated the use of the Texas Instrument (TI) Digital Micromirror Device (DMD) for various non-display applications including optical switching and imaging. In 2009, we proposed the use of the DMD to realize wavefront splitting interferometers as well as a variety of imagers. Specifically, proposed were agile electronically programmable wavefront splitting interferometer designs using a Spatial Light Modulator (SLM) such as (a) a transmissive SLM, (b) a DMD SLM and (c) a Beamsplitter with a DMD SLM. The SLMs operates with on/off or digital state pixels, much like a black and white state optical window to control passage/reflection of incident light. SLM pixel locations can be spatially and temporally modulated to create custom wavefronts for near-common path optical interference at the optical detectors such as a CCD/CMOS sensor, a Focal Plane Array (FPA) sensor or a point-photo-detector. This paper describes the proposed DMD-based wavefront splitting interferometer and imager designs and their relevant experimental results.

Keywords: Interferometer device, Imaging device, Spatial Light Modulator, Digital Micromirror Device.

1. INTRODUCTION

An optical interferometer is a powerful tool used in sensing, measurement and imaging applications. Ideally, an interferometer should be optically phase stable, operate over broadband spectrum (e.g., 350 nm to 2500 nm), and possess spatial and temporal programmability to enable the highest fringe contrast ratio optical interferometric detection. Because of its near common-path nature, the classical wavefront splitting interferometer is an ideal interferometer from a phase stability point-of-view [1-2]. One such wavefront splitting interferometer is the Young's double slit interferometer. Earlier, we have proposed and demonstrated the use of the Texas Instrument (TI) Digital Micromirror Device (DMD) for various non-display applications such as variable delay lines, optical switching, wavelength equalization, imaging, RF photonics, etc [3-33].

In 1997, we proposed using programmed gratings on the DMD to steer laser light [3]. More recently in 2009, we proposed the use of the DMD to realize wavefront splitting interferometers as well as a variety of imagers [34]. Very recently, this DMD-based Young's double slit interferometer design has been used to measure spatial coherence of a light source [35] and optical field values at a sample plane [36]. In this paper, we describe our proposed original SLM-based interferometer and imager designs and the basic experimental results by our Ref.34 DMD-based Young's double slit interferometer.

2. SLM-BASED WAVEFRONT SPLITTING INTERFEROMETER DESIGNS

Shown in Fig. 1 is the proposed agile electronically programmable wavefront splitting interferometer designs using a Spatial Light Modulator (SLM) such as (a) a transmissive SLM labelled in Fig. 1 with the number 855, (b) a DMD SLM labelled with the number 850 and (c) a Beamsplitter numbered 902 with a DMD SLM numbered as 950. Component numbering notation from the Ref.34 patent application is maintained to keep the originality of the dated works in Ref.34.

Optics, Photonics and Digital Technologies for Imaging Applications IV, edited by Peter Schelkens, Touradj Ebrahimi, Gabriel Cristóbal, Frédéric Truchetet, Pasi Saarikko, Proc. of SPIE Vol. 9896, 98960B · © 2016 SPIE · CCC code: 0277-786X/16/$18 · doi: 10.1117/12.2228373

These SLMs operates with on/off or digital state pixels, much like a black and white state optical window to control passage/reflection of incident light. Specifically, SLM pixel locations can be spatially and temporally modulated to create custom wavefronts for near-common path optical interference at an optical detector such as a CCD/CMOS sensor 805, a Focal Plane Array (FPA) sensor or a point photo-detector (PD). Fig. 1 (a) and (b) show classic Young's double slit (or point) implementations that generate fringes on the optical detection plane. These slit or point light sources on the DMD plane can be placed anywhere on its 2-D SLM plane and can also have different shapes and sizes to optimize fringe visibility.

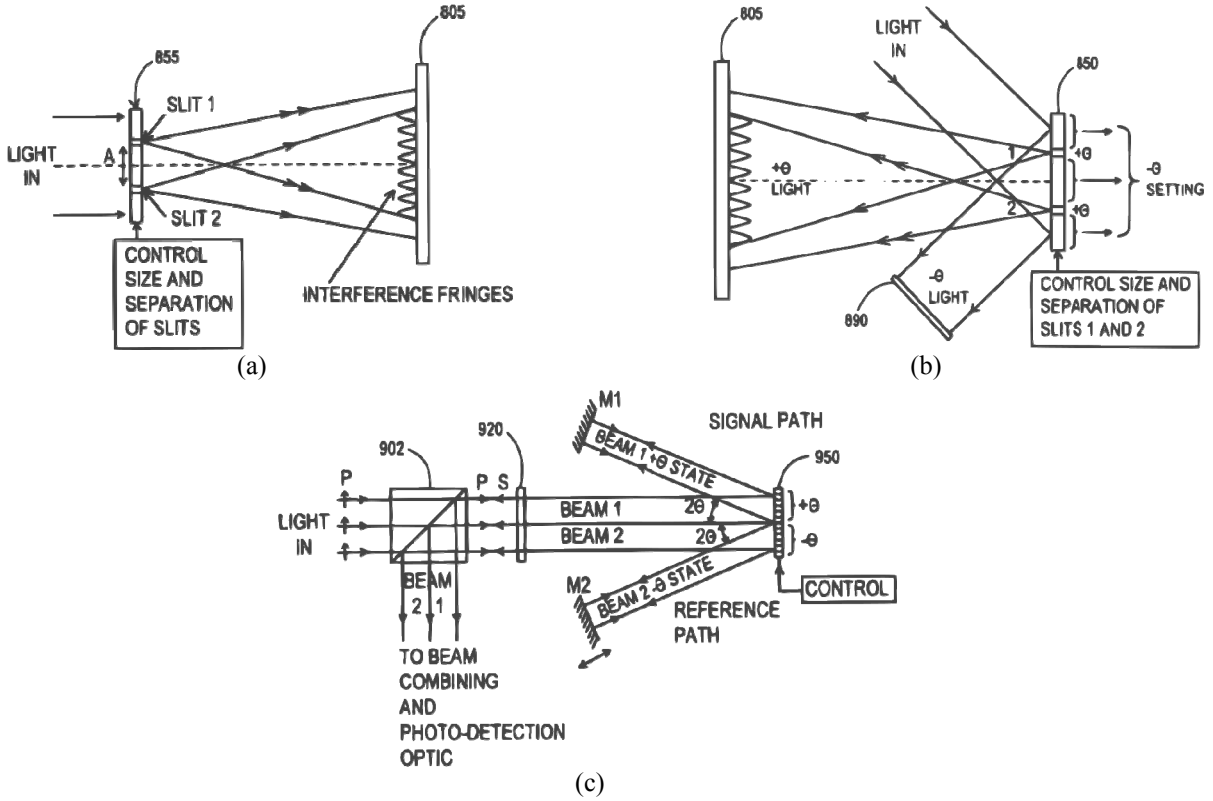

Fig. 1 Proposed agile electronically programmable wavefront splitting interferometer designs using a Spatial Light Modulator (SLM) such as (a) a transmissive SLM, (b) a DMD SLM and (c) a Beamsplitter with a DMD SLM.

It is well known that interferometry can not only be used to study the radiation in one of the paths of the interferometer but the system can also be used to study the coherence properties of the light source used to operate the interferometer. Fig. 1(c) shows a programmable wavefront splitting interferometer where a collimated horizontally or p-polarized light representing a full wavefront enters a Polarizing Beam Splitter (PBS) and then passes through a Quarter Wave Plate (QWP) to strike the DMD at normal incidence. The DMD is used to produce two separate wavefronts of programmable beam sizes. Each beam follows a separate beam path striking separate mirrors M1 and M2 with M1 in the interferometer signal path and M2 in the reference path. Reflected light from M1 and M2 strikes the DMD which redirects the reflected signal and reference light to the QWP and the PBS. Both light beams now being vertically or s-polarized get deflected by the PBS to enter beam combining and photo-detection optics. For example, the beam combining optics can be a lens and the photo-detection optics can be a point PD. Other types of beam combining optics can also be used such as a beam combining grating optic or a prism and mirror assembly, both engaged with 2-D CCD/CMOS sensor photo-detection. The mirror M2 can also be moved to produce phase shifts such as for scanned Fourier transform spectroscopy, for example, via a Lamellar grating produced by programming alternate pixels of the DMD, one pixel to go to M1 while the adjacent pixel is directed toward M2. Each 2 pixel beam can be combined on its return path via the DMD 950 with a lenslet array to form a multichannel interferometer. Note that it is not necessary that the two beams be side by side. Also, any wavefront division format can be delivered by programming the DMD to control beam powers, shapes, sizes and time duration.

3. EXPERIMENTAL DEMONSTRATION OF YOUNG'S DOUBLE SLIT INTERFEROMETER

The programmable Young's double slit interferometer is experimentally implemented in the laboratory using the different setups shown in Fig. 2. A 15 mW Melles Griot He-Ne laser having a wavelength of $\lambda = 633$ nm is used along with collimation optics comprising of a Newport microscope objective model MV-10x having numerical value of 0.25 and magnification of 10x, a 15 µm diameter pinhole aperture, and a collimation lens having a 20 cm focal length. The resulting collimated laser beam strikes the SLM at a normal incidence. In particular, the SLM used is the DLP3000 DMD chip which has a pixel pitch of 7.637 µm and a pixel count of 608 by 684 micromirrors that are arranged in a diamond shape structure. Each individual micromirror is programmable and can change its $\theta = \pm 12^{\circ}$ tilt orientation angle with respect to the DMD normal. To draw and display the agile Young's slits, the DMD chip is interfaced with a processor.

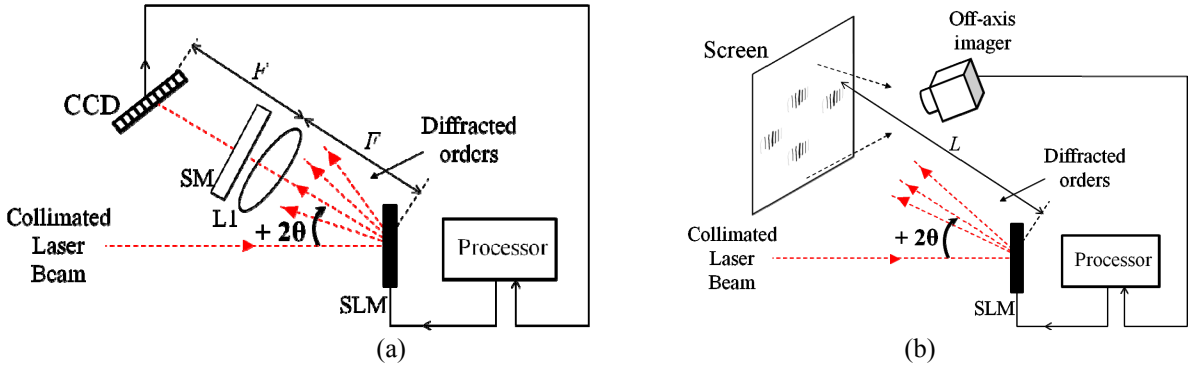

Fig. 2. Experimental optical designs used to demonstrate the proposed DMD-based Young's double slit interferometers.

In the first setup shown in Fig. 2(a), a convex lens L1 having focal length $F_{L1} = 5$ cm is located at a distance $F = F_{L1}$ from the SLM device and is positioned along the +2θ direction. Along the same direction, a target imaging plane represented by a CCD sensor is placed at a distance F from the lens L1. In such a configuration, the CCD plane represents the Fourier (spatial frequency) transform plane where the SLM is the signal space plane. Additional generic optical module, labelled as Smart Module (SM) as illustrated in Fig. 2(a) can be used in the proposed optical design if required. For instance, the SM component used for this experiment is an optical Neutral Density (ND) filter used to attenuate the light intensity that strikes the CCD sensor in order to avoid saturation issues. The second experimental setup of Fig. 2(b) does not use a capturing lens or CCD sensor. Instead, a target screen is deployed for visualization purposes located at a distance $L = 20$ cm away from the SLM device. An off-axis imager device is used to capture an instant screen shoot of the interference pattern on the screen. The imager deployed for the experiment is a commercial Nikon D3300 reflex camera.

A collimated laser beam striking the SLM generates diffraction orders due to the grating nature of the DMD chip. If two slits are displayed/ programmed on the SLM, each of the orders diffracted in the +2θ direction contain a corresponding interference pattern due to diffraction at the slits. Such interference patterns can be visualized directly on a CCD sensor as in Fig. 2(a) or on the screen as in Fig. 2(b). It is important to note here that there are two sets of diffraction occurring simultaneously. One is due to the grating nature of the DMD and the other is due to presence of programmable slits. In this experiment, the latter, i.e., the interference due to the slits, is of interest.

The flexibility and programmability of the DMD chip deployed as the SLM allows different degrees of freedom in terms of slit dimensions, slit shape, slit separation distance, slit orientation, and number of slits to use. First, the Fig. 2(a) setup is implemented in the laboratory. Fig. 3 shows a representation of the slits displayed on the DMD and its corresponding interference pattern on the CCD sensor obtained when the slit separation distance d is equal to 64.8 µm (Fig. 3(a)) and 129.6 µm (Fig. 3(b)). The thickness of each slit is 21.6 µm. It can be seen in Fig. 3 that the location of the diffraction orders due to the grating nature of DMD chip stay the same, but only the interference pattern within each of these orders changes when the slit separation d is changed.

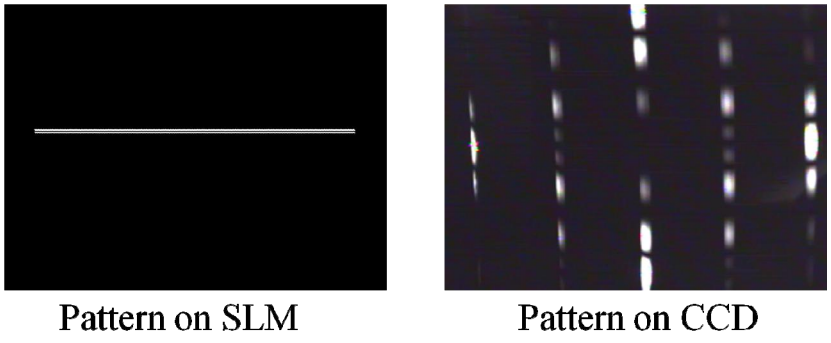

(a)

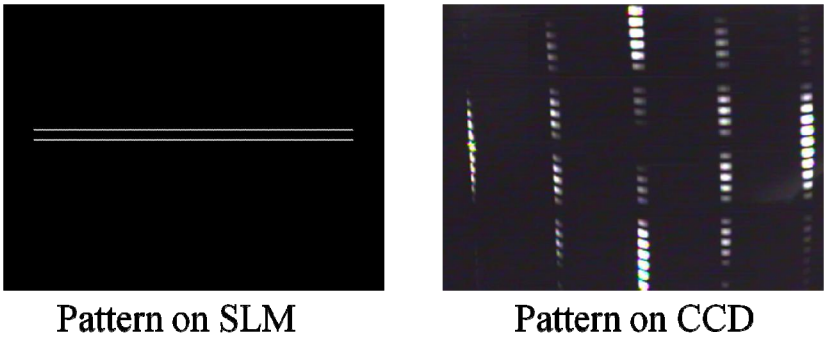

(b)

Fig. 3. (a) (left) Computer generated image of a double slit that is transferred onto the DMD chip to create two horizontal slits separated by 64.8 μm and the (right) corresponding far-field interference pattern produced on the CCD sensor when a 633 nm collimated laser beam is incident on DMD chip. (b) (left) Computer generated image of double slit that is transferred onto the DMD chip to create 2 horizontal slits separated by 129.6 μm and the (right) corresponding far-field interference pattern produced on the CCD sensor when a 633 nm collimated laser beam is incident on DMD chip.

Next, the Fig. 2(b) setup is deployed. Here, the DMD chip is programmed to display slits having d values of 61.09 μm, 122.19 μm, 183.29 μm and 244.38 μm. The thickness (i.e., width) of each slit is 30.55 μm. Due to the diamond arrangement of the micromirrors on the DMD chip, the programmed slits deployed are oriented following the natural DMD chip structure, i.e. are diagonally oriented at 45˚ angle from the DMD chip horizontal. Both slit orientations of +45˚ and -45˚ are used.

The following equation to evaluate the fringe separation is deployed for the analysis of the Fig. 2(b) setup [37]:

$$\lambda = \frac{xd}{nL} \tag{1}$$

where λ is the wavelength of the light source, x represents the distance from the central fringe (which is the one containing the zeroth-order associated to the brightest diffraction spot), d is the distance between the slits displayed in the SLM device and n is the order of the fringe.

The Fig. 2(b) experimental setup results are displayed in Fig. 4. Fig. 4(a) shows a completely blank pattern programmed on SLM with all micromirrors reflecting light towards the +2θ direction and its corresponding off-axis view of the interference pattern striking the screen. Note that this diffraction pattern is only due to the grating nature of the DMD. A ruler is positioned on the screen to aid subsequent measurements. Notice that subsequent interference pattern will appear at each of the order location shown in Fig. 4(a) when slits are programmed on the DMD. Fig. 4(b) shows the

programmed diagonally oriented double slit at +45˚ on the SLM having d = 61.09 μm and its corresponding interference pattern on the screen. As expected, an interference pattern due to the programmed double slit is present in each diffraction order of the DMD grating diffraction pattern. Fig. 4(c) shows the programmed diagonally oriented double slit at +45˚ on the SLM having d = 247.38 μm and its corresponding interference pattern on the screen.

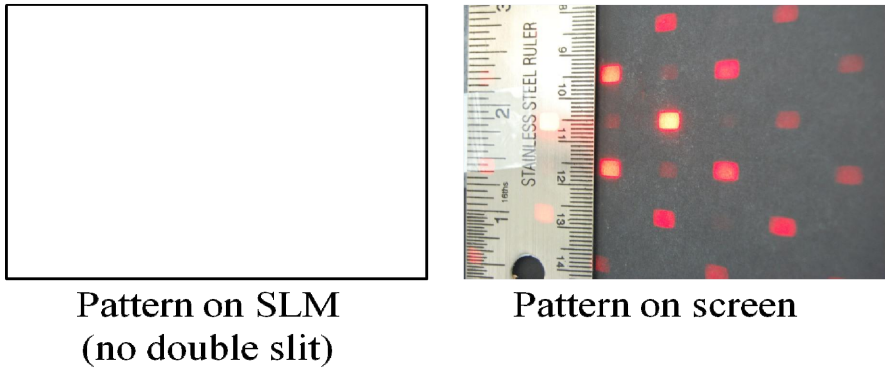

(a)

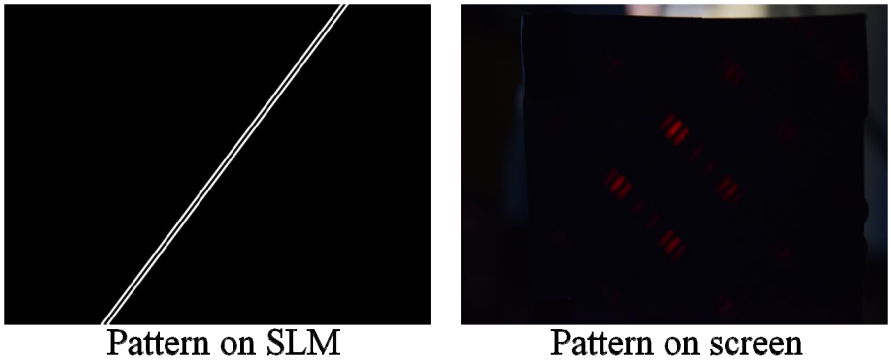

(b)

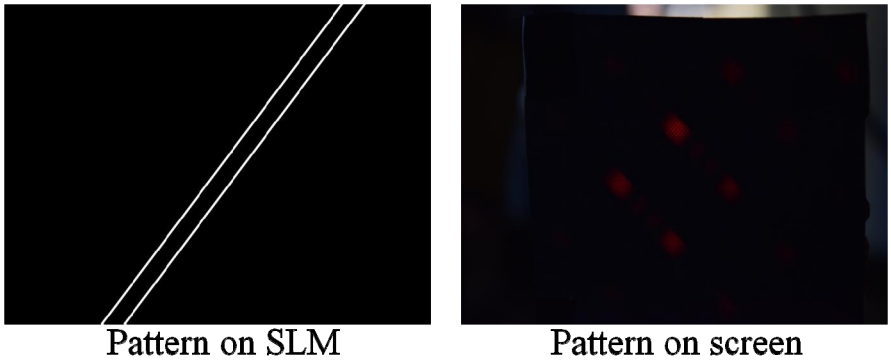

(c)

Fig. 4. (a) (left) Computer generated image transferred onto the DMD chip representing all the micromirrors that deviates the light towards the screen direction to visualize on screen the diffraction order spots (right).(b) (left) Computer generated image of double slit that is transferred onto the DMD chip to create two diagonally oriented slits at +45˚ separated by 61.09 μm and the (right) corresponding far-field interference pattern produced on the CCD sensor when a 633 nm collimated laser beam is incident on DMD chip. (c) (left) Computer generated image of double slit that is transferred onto the DMD chip to create two diagonally oriented slits at +45˚ separated by 247.38 μm and the (right) corresponding far-field interference pattern produced on the CCD sensor when a 633 nm collimated laser beam is incident on DMD chip.

From the experimental findings and by using Eqn. (1), a comparison is conducted between the theoretical fringe spacing x_{th} and the actual experimental fringe spacing x_{exp} for both diagonal orientations. This comparison is summarized in Table 1.

Table 1 Experimental versus theoretical fringe separation.

Slit Separation d [μm]	Theoretical Fringe spacing x_{th} [mm]	Experimental fringe spacing x_{exp}, $+45^{\circ}$ [mm]	Experimental fringe spacing x_{exp} -45° [mm]
61.09	2.0721	2.1587	2.1746
122.19	1.0361	1.1429	1.0794
183.29	0.6907	0.7619	0.6984
244.38	0.5180	0.5873	0.5397

The results shown in Table 1 prove the effectiveness of the programmable SLM device as a programmable Young's double slit interferometer even though the uncertainty error introduced by the measuring tool is evident when increasing the slit separation distance d. Specifically one notes that the fringe separation decreases, enlarging the uncertainty of the fringe separation measurement.

4. IMAGING USING 3-D SCANNING APERTURES

As shown in Fig. 5 and described earlier [38-40], Three Dimensional (3-D) optical scanners with a laser object illumination source and a single-point detector including the use of optical amplification in the signal processing Transmitter/Receiver chain can be used for active or laser-based imaging of 3-D objects. Here an Electronically Controlled Variable Focus Lens (ECVFL) can be used to electronically translate a scanning pixel along the light propagation axis providing for 3-D image depth information.

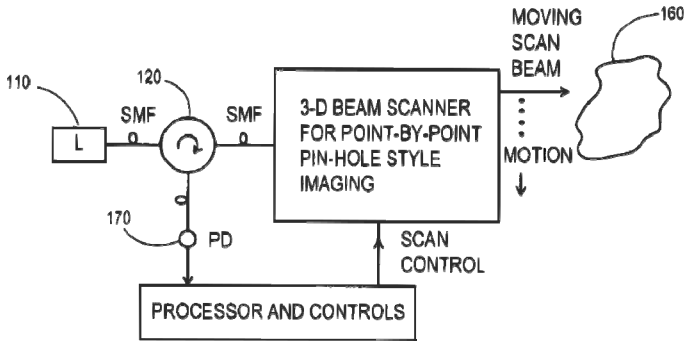

Fig. 5. Block diagram of a 3-D imager design using electronic beam 3-D scan/position controls and a single point photo-detector and optical illumination source.

Fig. 6(a) and Fig. 6(b) show the module design for implementing a smart camera for 3-D imaging via single point photo-detection and with focus and aperture size control via an ECVFL-SLM combination. The cascaded ECVFL 420 and DMD 450 devices are engaged within a novel design to deliver the powers of a specific application, in this case, a 3-D imager. As shown in Fig. 6(a), various transverse image planes at different axial directions (along beam direction) of a 3-

D object 460 are imaged on to the DMD plane using a cascade of a fixed lens 430 and the ECVFL 420. Thus, by changing the ECVFL focal length by electronic control 440, a sequence of 2-D images of the object 460 at different axial depths (along the optic-axis of the system) are acquired using pin-hole profiling control of the DMD 450 and the focus/beam collection lens 433 and the single large area point photo detector 470. Thus, the DMD forms a moving pin-hole on the projected 2-D image plane/DMD plane where the object 2-D image occurs for a given axial/depth position of the 3-D object 460.

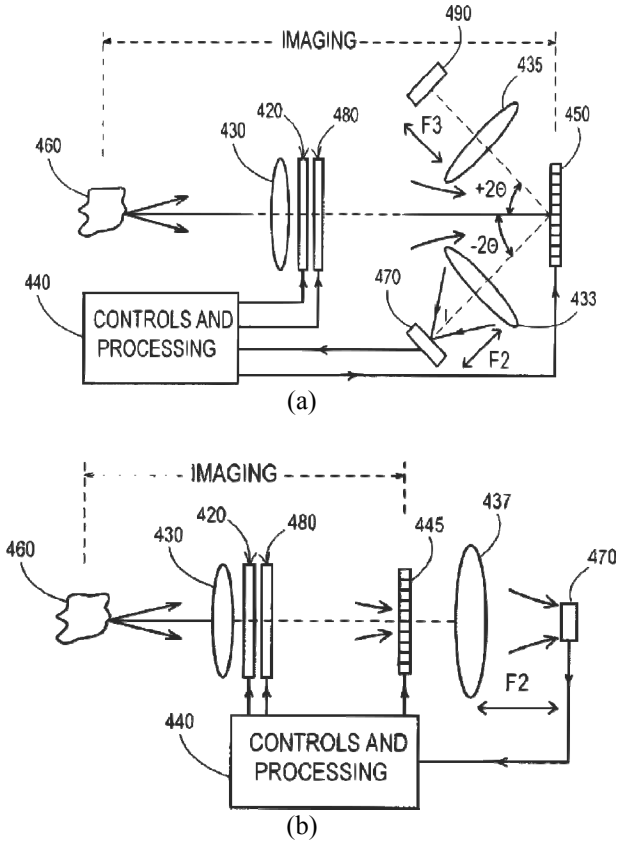

Fig. 6. Schematic block diagram of a module for implementing smart camera for 3-D imaging with focus and aperture size control via an ECVFL-SLM combination and single point photo-detection. Options of (a) Reflective SLM and (b) Transmissive SLM.

The distance between focus/beam collection lens 433 and photo detector 470 is the focal length F2 of focus/beam collection lens 433. Object light enters at normal incidence on the DMD so the object image forms on the flat DMD plane, ideal for pin-hole sampling of the object 2-D image at a given ECVFL focus. The DMD 450 has ± θ state micromirrors. As shown, the pinhole is formed by assigning the –θ state to a select number of micromirrors in a given zone on the DMD 450 so that selected light from the object image is directed to focus/beam collection lens 433 where all this light is captured by photo detector 470 to represent light from a given part of the image zone. All the other micromirrors are set to the +θ state so all this light off the projected object image is directed to focus/beam collection lens 435 and physically blocked by a spatial block 490. A color filter 480 cascaded to the ECVFL 420 can be used to sample object image data on a per color (e.g., red, green, blue) basis. Spatial block 490 can be an electronically controlled LC color filter.

As the DMD 450 can be programmed by an electronic controller 440, the pinhole on the projected image can be made to move across the entire image to form a 2-D point sampler, thus having photo detector 470 produce point-by-point object irradiance data that can be used by the processing electronics 440 to reconstruct the given 2-D image slice. Given the

ECVFL varies its focus, plural object 2-D image slices can be reconstructed to make a 3-D image of object 460 and hence realize a 3-D camera. The smallest pin-hole size is a single micromirror while bigger pinhole sizes and needed shapes can be used depending on the object type and imaging quality needed.

Fig. 6(b) shows a transmissive 3-D camera module design using a liquid crystal LC SLM 445 instead of the DMD shown in Fig. 6(a) although the working principles are similar. In this case, light entering the system is linearly polarized for proper LC SLM operations. Typically, the LC SLM 445 consists of two polarizers with LC material layer sandwiched in-between so that no separate external polarizer is needed in some cases of LC SLMs. In this embodiment, the entire 3-D camera is controlled by an electronic controller 440 for optical power detection by the photodetector 470, SLM 445, color filter 480, and ECVFL control, and image processing at the processing and controller electronics 440.

A typical SLM can have 1 million pixels implying 1 million pin-holes can sample a typical projected image falling on the flat SLM surface. Typically, pixels are square or rectangular design, so one can program the SLM to form a variety of pinhole shape such as hexagons, circles, ellipses, etc, to form the point-sampling head/delta function. Fixed lens 430 can be replaced by a mechanically spinning head containing a variety of fixed but different focal length lenses to give more focus power to the 3-D camera module.

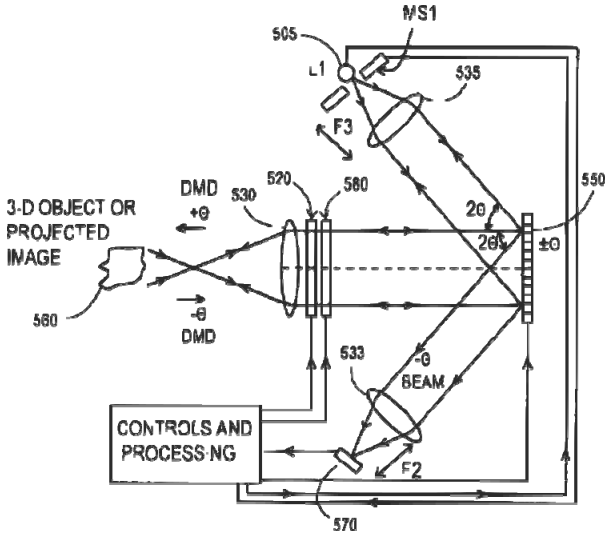

Fig. 7. Schematic block diagram of a module for implementing combined projector and camera module for 3-D imaging with single point photo-detection.

Fig. 7 is a schematic diagram showing the module for implementing combined projector and camera module for 3-D imaging with single point photo-detection. The basic design is the same as Fig. 6, except the spatial block 490 is replaced by a light source L1 505 that feeds the DMD projection system. To act as a DMD image projector, a digital image is fed to the DMD 550. Light for projection that carries the chosen image is directed through the path containing the imaging lens combination of fixed lens 530 and ECVFL 520. To generate a 3-D image, one can change the ECVFL focal length to a direct image plane in the 3-D object plane.

To actually see a 3-D object, the image planes must get independently illuminated such as via use of a special material that lights up when in this in-focus image plane. To send light through the image projection path, the DMD 550 micromirrors need to be set to their $+\theta$ state, and any $-\theta$ state indicates dark parts of the projected image that occur as light is rejected and sent into the collection lens 533 arm where it is collected by photo detector 570. In this projector operation case, photo detector 570 output is inactive or not used for processing. The color filter 580 is set in sequence to the appropriate colors for each image on the DMD 550 to complete the color projection operation.

Alternatively, the color filter 580 can be removed and use three separate color sources in parallel with independent time modulation to generate the design color for the image. To operate the Fig. 7 module as a 3-D camera, the light source 505 is turned off and photo detector 570 is turned on to collect the light from the image on the DMD 550 with the DMD

operated as a scanning pin-hole to sample the image point-by-point as done in the Fig. 6 camera module. The rejected light is directed to collection lens 535 and falls on L1 505. One can also deploy a mechanical shutter MS1 in front of the L1 505 to act as a beam block like spatial block 490 in Fig. 6. Thus, the module forms both a 3-D camera and a 3-D image projector. In its basic mode with ECVFL inactive, the module forms both a 2-D camera via a point detector and a 2-D image projector.

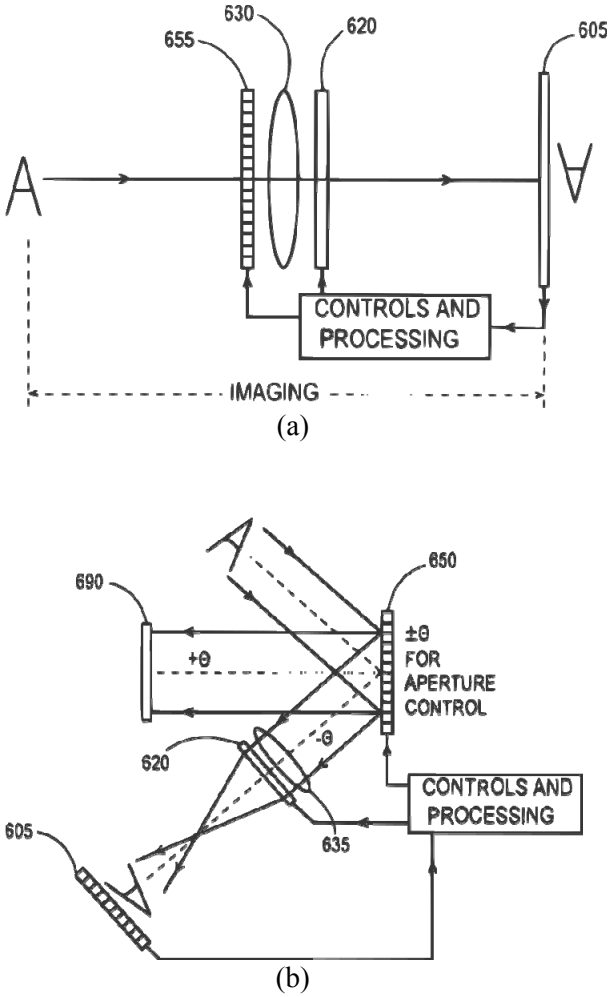

Fig. 8. Schematic block diagram of a module for implementing a lens-based aperture controlled camera with a digital 2-D SLM and 2-D detector array.

Fig. 8(a) and 8(b) shows the proposed module for implementing a classic lens-based aperture controlled camera with a digital 2-D SLM and 2-D detector array. Fig. 8(a) uses a transmissive LC SLM 655 cascaded with a fixed imaging lens 630 and an ECVFL 620. The SLM 655 produces a controlled aperture for the imaging camera 605 to control light throughput. The ECVFL 620 provides image focus control. Fixed lens 630 with the ECVFL 620 acts as the imaging lens that transfer the object plane to the CCD imager plane. The CCD 605 is a 2-D detector array. Fig. 8(b) shows a similar aperture controlled camera module as Fig. 8(a) apart from the fact that the SLM 655 is a reflective DMD 650 and the optical design is reflective.

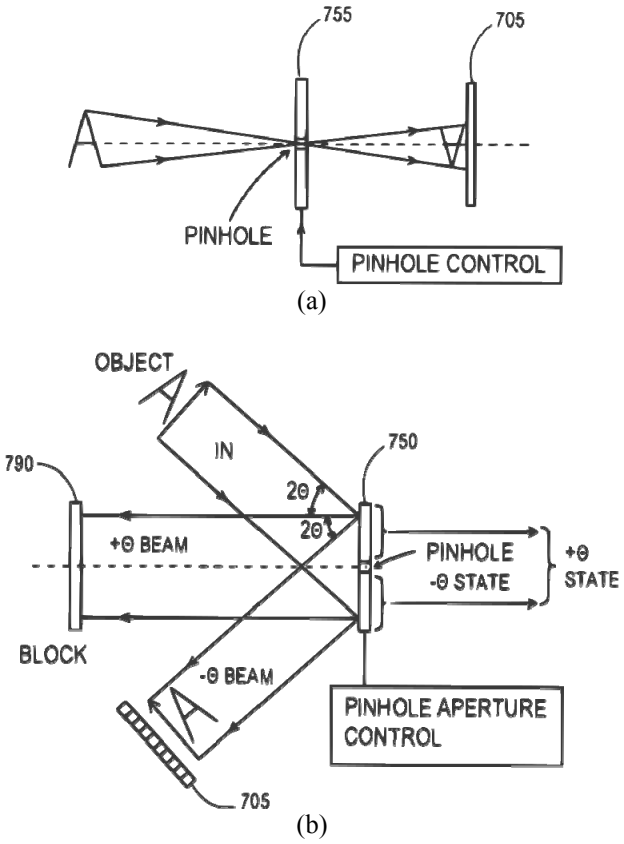

Fig. 9. Schematic block diagram of a module for implementing a lens-less pinhole camera with a digital 2-D SLM and 2-D detector array.

Fig. 9 is a schematic diagram showing the module for implementing a classic lens-less pinhole camera with a digital 2-D SLM and 2-D detector array. Unlike the Fig. 8(a) and 8(b) modules, the Fig. 9(a) and 9(b) configurations contain no lens for imaging. The imaging operation is produced by using the LC SLM 755 as a controlled size pinhole at the center of the SLM 655, making a classic Al-Hazen pinhole camera, but with an electronically programmable pinhole size to produce the best quality image in terms of focus, Field-of-View, etc. The Fig. 9(a) lens-less pinhole camera module uses a LC SLM 755 and CCD 705 while the Fig. 9(b) module design includes a DMD 750, CCD 705, and spatial block 790. The LC SLM 755 has polarizers, much like a LC display to act a light on/off shutters on a SLM pixel basis. The DMD 750 uses the –θ state of micromirrors to represent the pinhole that then directs the light coming from the object to travel to the CCD 705. The remaining micromirrors are set to the +θ state to send light away from the CCD 705 and to the light block 790.

Do note that for all the presented modules that use timed photo-detection to integrate light, the DMD can also operate as a timed on/off shutter due to its fast programming speeds. Hence, apart from controlling the speed of the photo-detector integration times, the DMD can also be engaged to modulate the light signals in time to produce powerful image processing effects.

5. CONCLUSION

Proposed is the design of a programmable SLM-based wavefront splitting interferometer such as a Young's double slit interferometer. Using the DMD as the SLM, demonstrated is a programmable Young's double slit interferometer that offers complete programmability over slit properties such as slit size, slit shape, slit width, slit time and number of slits. Other advantages of the demonstrated interferometer are its 100% spatial repeatability of the slits and the ability for the

DMD to handle high power broad spectrum incident light. Given the demonstrated interferometer's cost effectiveness and operational reliability, it can serve as a demonstration unit for optics education in schools and universities. The paper has also presented several imager designs using 3-D scanning apertures. Specifically, these imager designs are empowered by using a combination of components including SLMs, ECVFLs, lenses, apertures, colour filters, CCD/CMOS sensors, and single point photo-detectors. Future work relates to the design and experimental demonstration of the proposed design modules for agile interferometry and imaging.

REFERENCES

[1] M. Francon, Optical Interferometry, Academic Press, New York & London, 1966.
[2] P. Hariharan, Optical Interferometry, Academic Press, San Diego & London, 2003.
[3] N. A. Riza, "Coherent techniques and deformable-mirror device (DMD)-based switched photonic time delay control for high frequency antenna arrays," SPIE Conf. on Optical Technology for Microwave Applications VIII, Vol.3160, pp.97-105, San Diego, August 1997.
[4] N. A. Riza and S. Sumriddetchkajorn, "Fault Tolerant Dense Multi-Wavelength Add/Drop Filter using a Two Dimensional Digital Micromirror Device," Applied Optics-LP, Vol. 37, Issue 27, Page 6355, September 1998.
[5] N. A. Riza and S. Sumriddetchkajorn, "Fault tolerant polarization insensitive photonic delay line architectures using Two Dimensional Digital Micromirror Devices," Optics Communications, Vol. 160, pp.311-320, 15 Feb., 1999.
[6] N. A. Riza and S. Sumriddetchkajorn, "Digitally controlled fault tolerant multiwavelength programmable fiber-optic attenuator using a two dimensional digital micromirror devices," Optics Letters, Vol. 24, Issue 5, Page 282, March 1, 1999.
[7] N. A. Riza and S. Sumriddetchkajorn, "Small Tilt Micromirror Device-based Multiwavelength Three Dimensional 2 □ 2 Fiber-Optic Switch Structures," Optical Engineering, Vol.39, No.2, pp.379-386, Feb. 2000.
[8] N. A. Riza and S. Sumriddetchkajorn, "Micromechanics-based wavelength-sensitive photonic beam control architectures and applications," Applied Optics, Vol. 39, No. 6, pp. 919-932, 20 Feb. 2000.
[9] S. Sumriddetchkajorn and N. A. Riza, "Fault-tolerant three-port fiber-optic attenuator using small tilt micromirror device," Optics Communications, pp. 77-86, April 2002.
[10] S. Sumriddetchkajorn and N. A. Riza, "Micro-Electro-Mechanical System-Based Digitally Controlled Optical Beam Profiler," Applied Optics-LP, Vol. 41, Issue 18, Page 3506, June 2002.
[11] N. A. Riza and M. J. Mughal, "Broadband optical equalizer using fault tolerant digital micromirrors," Optics Express Internet Journal, Vol. 11, pp.1559-1565, June 30, 2003.
[12] N. A. Riza and M. A. Arain, "Programmable Broadband Radio-Frequency Transversal Filter with Compact Fiber-Optics and Digital Microelectromechanical System-Based Optical Spectral Control," Applied Optics, Vol.43, No.15, pp.3159-3165, May 2004.
[13] N. A. Riza and F. N. Ghauri, "Hybrid Analog Digital MEMS Fiber Optic Variable Attenuator," IEEE Photonic Technology Letters, Vol.17, No.1, pp. 124-126, Jan. 2005.
[14] N. A. Riza and F. N. Ghauri, "Super resolution variable fiber-optic attenuation instrument using digital micromirror device," AIP Review of Scientific Instruments Journal, Vol.76, No.1, 2005.
[15] N. A. Riza and F. N. Ghauri, "Super Resolution Hybrid Analog-Digital Optical Beam Profiler Using Digital Micro-Mirror Device," IEEE Photon. Tech. Lett., Vol. 17, No.7, pp.1492-94, July 2005.
[16] M. A. Arain and N. A. Riza, " Optoelectronic approach to adaptive radio frequency transversal filter implementation with negative coefficients by using optical spectrum shaping," Applied Optics, Vol.45, No.11, 10 April 2006.
[17] S. A. Khan and N. A. Riza, "Demonstration of a MEMS Digital Micromirror Device-based broadband reconfigurable optical add-drop filter for dense wavelength division multiplexing systems," IEEE/OSA Journal of Lightwave Technology, 2006.
[18] N. A. Riza and S. A. Reza, "Hybrid analog-digital design microelectromechanical systems spectral processor for simultaneous gain slope and channel equalization controls," Optical Engineering, Vol.46, No.3, March 2007.
[19] N. A. Riza and S. A. Reza, "Smart Value-Added Fiber-Optic Modules using Spatially Multiplexed Processing," Applied Optics, Vol.46, No.18, pp.3800-3810, June 2007.

[20] N. A. Riza and S. A. Reza, "Broadband All-Digital Variable Fiber-Optic Attenuator using Digital Micro-Mirror Device," IEEE Photon. Tech. Lett., Nov.1, 2007.
[21] N. A. Riza and F. N. Ghauri, "High Resolution Tunable Microwave Filter using Hybrid Analog-Digital Controls via an Acousto-Optic Tunable Filter and Digital Micromirror Device," IEEE/OSA Journal of Lightwave Technology, Vol.26, No.17, Sept.1, pp.3056-3061, 2008.
[22] N. A. Riza and S. A. Reza, "High-dynamic-range hybrid analog–digital control broadband optical spectral processor using micromirror and acousto-optic devices," Optics Letters, Vol. 33, pp.1222-1224, May 2008.
[23] M. Sheikh and N. A. Riza, "Demonstration of Pinhole Laser Beam Profiling using a Digital Micromirror Device," IEEE Photon. Tech. Lett., Vol.21, May 15, 2009.
[24] S. A. Reza and N. A. Riza, "High Dynamic Range Variable Fiber Optical Attenuator using Digital Micromirrors and Opto-fluidics," IEEE Photon. Tech. Lett., Vol.21, July 2009.
[25] M. Sheikh and N. A. Riza, "Motion-Free Hybrid Design Laser Beam Propagation Analyzer using a Digital Micro-mirror Device and a Variable Focus Liquid Lens," Applied Optics, June 2010.
[26] N. A. Riza, S. A. Reza and P. J. Marraccini, "Digital micro-mirror device-based broadband optical image sensor for robust imaging applications," Optics Communications 284, 1, 2011.
[27] P. J. Marraccini and N. A. Riza, Multimode Laser Beam Analyzer Instrument using Electrically Programmable Optics," AIP Rev. Scientific Instruments Journal, Vol.82, 2011.
[28] N. A. Riza, P. J. Marraccini, and Cody Baxley, " Data Efficient Digital Micromirror Device-Based Image Edge Detection Sensor using Space-Time Processing," Vol.12, No.5, p.1043-1047, May 2012.
[29] N. A. Riza, "Application intelligence-based Imaging using programmable photonics," Photonics Ireland Conference Proc., Belfast, Sept. 2013 (Invited Paper).
[30] J. P. La Torre, M. J. Amin, M. Magno and N. A. Riza, "An Embedded Smart Agile Pixel Imager for Lasers," 6th European Embedded Design in Education and Research Conference (EDERC), pp.230-234, 11-12 Sept. 2014.
[31] M. J. Amin, J. P. La Torre, N. A. Riza, "Embedded Optics and Electronics Single Digital Micromirror Device-based Agile Pixel Broadband Imager and Spectrum Analyser for Laser Beam Hotspot Detection," Applied Optics, Vol. 54, pp. 3547–3559, 2015.
[32] N. A. Riza, M. J. Amin, J. P. La Torre, "Coded Access Optical Sensor (CAOS) Imager," Journal of the European Optical Society (JEOS) Rapid Publications, Vol. 10, 15021, April 2015.
[33] N.A. Riza and P.J. Marraccini, "Programmable optic-based robust underwater/free-space optical data transfer link designs for applications using high power lasers," Photonics Ireland Conference Proceedings, Sept. 2015.
[34] N. A. Riza, "Agile optical image sensing, control, and measurement modules," USA Patent Application No. 61/258,344, 2009.
[35] H. Partanen, J. Turunen, and J. Tervo, "Coherence measurement with digital micromirror device," Optics Letters, Vol. 39, No. 4, February 15, 2014.
[36] G. Vdovin, H Gong, O Soloviev, P Pozzi and M Verhaegen, "Lensless coherent imaging by sampling of the optical field with digital micromirror device," UK IOP Journal of Optics, Vol. 17, 122001, pp.1-5, Oct. 8, 2015.
[37] E, Hecht, Optics, 4th Edition, Pearson, 2002.
[38] N. A. Riza, "BOPSCAN technology: A methodology and implementation of the billion point optical scanner," Proc. SPIE 3482, International Optical Design Conference (IODC), 572, September 1998.
[39] N. A. Riza and Yu Huang, "High speed optical scanner for multi-dimensional beam pointing and acquisition," in LEOS IEEE Annual Meeting Conf. Proc., Vol.1, pp.184-185, 1999.
[40] N. A. Riza, "Multiplexed optical scanner technology," Patent No. 6 687 036, Feb. 3, 2004.